Title
Global estimates of mineral dust aerosol iron and aluminum solubility that account for particle size using diffusion-controlled and surface-area-controlled approximations

Journal
Global Biogeochemical Cycles, 26(2)

ISSN
08866236

Authors
Han, Qin
Zender, Charles S
Moore, J. Keith
et al.

Publication Date
2012-06-01

DOI
10.1029/2011GB004186

Peer reviewed

Global estimates of mineral dust aerosol iron and aluminum solubility that account for particle size using diffusion-controlled and surface-area-controlled approximations

Qin Han,[1] Charles S. Zender,[1] J. Keith Moore,[1] Clifton S. Buck,[2] Ying Chen,[3] Anne Johansen,[4] and Christopher I. Measures[5]

Received 18 August 2011; revised 19 April 2012; accepted 7 May 2012; published 20 June 2012.

[1] Mineral aerosol deposition is recognized as the dominant source of iron to the open ocean and the solubility of iron in the dust aerosol is highly variable, with measurements ranging from 0.01–80%. Global models have difficulty capturing the observed variations in solubility, and have ignored the solubility dependence on aerosol size. We introduce two idealized physical models to estimate the size dependence of mineral aerosol solubility: a diffusion-controlled model and a surface-area-controlled model. These models produce differing time- and space-varying solubility maps for aerosol Fe and Al given the dust age at deposition, size-resolved dust entrainment fields, and the aerosol acidity. The resulting soluble iron deposition fluxes are substantially different, and more realistic, than a globally uniform solubility approximation. The surface-area-controlled solubility varies more than the diffusion-controlled solubility and better captures the spatial pattern of observed solubility in the Atlantic. However, neither of these two models explains the large solubility variation observed in the Pacific. We then examine the impacts of spatially variable, size-dependent solubility on marine biogeochemistry with the Biogeochemical Elemental Cycling (BEC) ocean model by comparing the modeled surface ocean dissolved Fe and Al with observations. The diffusion-based variable solubility does not significantly improve the simulation of dissolved Fe relative to a 5% globally uniform solubility, while the surface-area-based variable solubility improves the simulation in the North Atlantic but worsens it in the Pacific and Indian Oceans.

Citation: Han, Q., C. S. Zender, J. K. Moore, C. S. Buck, Y. Chen, A. Johansen, and C. I. Measures (2012), Global estimates of mineral dust aerosol iron and aluminum solubility that account for particle size using diffusion-controlled and surface-area-controlled approximations, *Global Biogeochem. Cycles*, *26*, GB2038, doi:10.1029/2011GB004186.

1. Introduction

[2] Iron is a critical nutrient for organisms in the ocean and thus has an important impact on the ocean biogeochemical cycles and the global carbon cycle. Iron deficiency limits the primary production in High-Nutrient Low-Chlorophyll (HNLC) ocean regions [*Martin and Fitzwater*, 1988; *Behrenfeld et al.*, 1996; *Boyd et al.*, 2000]. In the remote oceans, atmospheric transport and deposition is a key source of iron to the surface waters [*Fung et al.*, 2000; *Jickells and Spokes*, 2001]. Numerous modeling and experimental studies have investigated the concentration, deposition and solubility of atmospheric aerosols. However, the bio-available iron deposition is still not well known and more studies on aerosol iron solubility are required [*Jickells et al.*, 2005].

[3] Aluminum, on the other hand, is not found to be an important nutrient but is a useful tracer for crustal material [*Arimoto et al.*, 2003]. However, due to its special geochemical characteristics, e.g. common and relatively invariant content (~8%) over the Earth's crust [*Wedephohl*, 1995], relatively short residence time (~6.5 yr) in the surface ocean [*Jickells et al.*, 1994] and relatively simple chemistry compared to Fe, aluminum has been used as a tracer for quantifying the dust deposition to the surface ocean [*Measures and Vink*, 2000; *Han et al.*, 2008]. *Han et al.* [2008] ignored the spatial variation of mineral dust solubility and treated Al solubility as size-independent.

[4] Iron in mineral dust is not very soluble (~0.5%) in source regions [*Fung et al.*, 2000] and usually becomes more soluble by the time of deposition. The reported atmospheric iron solubility spans over three orders of magnitude (0.01%–80%) [*Mahowald et al.*, 2005]. *Shi et al.* [2011b] simulated

[1]Department of Earth System Science, University of California, Irvine, California, USA.
[2]Department of Oceanography, Florida State University, Tallahassee, Florida, USA.
[3]Department of Environmental Science and Engineering, Fudan University, Shanghai, China.
[4]Chemistry Department, Central Washington University, Ellensburg, Washington, USA.
[5]Department of Oceanography, University of Hawai'i at Mānoa, Honolulu, Hawaii, USA.

Corresponding author: C. S. Zender, Department of Earth System Science, University of California, Irvine, CA 92617, USA. (zender@uci.edu)

acid processes in the atmosphere and measured the potential Fe solubility of dust precursor samples from North African dust source regions to vary from 0.7% to 17.3%. Fewer Al solubility measurements are available but existing data also show strong spatial variations (0.5%–86%) [*Prospero et al.*, 1987; *Baker and Jickells*, 2006; *Buck et al.*, 2006, 2008b; *Measures et al.*, 2010]. Atmospheric processes seem to increase mineral aerosol iron solubility during transport from source regions to the open oceans [*Jickells and Spokes*, 2001; *Mahowald et al.*, 2005]. Several solubilizing mechanisms have been proposed including processing by natural and anthropogenic organic acids [*Zuo and Holgné*, 1992; *Siefert et al.*, 1994] and by sulfate and nitrate coatings [*Zhuang et al.*, 1992; *Zhu et al.*, 1992] that, along with photochemical processing, occurs both within and outside of clouds [*Jickells and Spokes*, 2001; *Hand et al.*, 2004; *Johansen and Key*, 2006]. It has also been proposed that soluble iron has large combustion sources including biomass burning [*Chen and Siefert*, 2004; *Chuang et al.*, 2005] and combustion of heavy fuel oil [*Sholkovitz et al.*, 2009]. There is evidence that mineralogical changes in Fe speciation (e.g., due to combustion) are important in determining solubility [*Shi et al.*, 2009, 2011a]. *Sholkovitz et al.* [2009] also discussed the physical mixing of chemically distinct aerosol populations at Bermuda and the affect on observations of aerosol iron solubility. Unfortunately, global models based on these mechanisms have difficulty predicting the observed solubility [*Hand et al.*, 2004; *Luo et al.*, 2005; *Fan et al.*, 2006; *Luo et al.*, 2008].

[5] *Baker and Jickells* [2006] argue that the control of Fe solubility is primarily physical rather than chemical in nature. They find a positive correlation between solubility and the surface area to volume ratio of dust particles. Observations show enrichment of labile Fe in fine aerosol samples compared to coarse aerosols [*Siefert et al.*, 1999; *Johansen et al.*, 2000; *Chen and Siefert*, 2004]. On the other hand, *Hand et al.* [2004] suggested that the prolonged acid and photochemical processing of fine particles could be responsible for their higher Fe solubility relative to larger particles which have a shorter atmospheric lifetime. Thus the globally uniform, size-independent, constant Al solubility used by *Han et al.* [2008] is unrealistic and may contribute to the model-observation discrepancies.

[6] In this work, we develop two distinct conceptual models of mineral aerosol solubility based on diffusion-controlled dissolution and surface-area-controlled dissolution, respectively. These models estimate solubility as a function of particle size, atmospheric transport time, and aerosol acidity. Using the particle size distribution, acid deposition flux and aerosol age predicted by global models, we produce two global solubility maps and apply them to an ocean ecosystem model. The model results allow us to evaluate the simulated sensitivity of aerosol solubility to particle size, and to test each conceptual model for advantages in simulating the observed distribution of dissolved Fe and Al.

2. Methods

2.1. Conceptual Model I: Classical Diffusion-Controlled Dissolution

[7] Chemical diffusion occurs when there is a gradient in chemical potential, which is generally described by Fick's first law. In solid-Earth systems, several diffusion pathways exist in rocks as well as in individual mineral grains. The diffusivity of mineral grains may depend upon the presence of fast pathways—extended defects in the crystal lattice, which are migrations along extended intracrystalline defects such as dislocations. Water condenses to a particle's surface soon after it encounters air with relative humidity (RH) ≥20% [*Grassian*, 2001]. The dissolution of dust particles begins immediately on contact with a liquid coating like water. From the view of classical diffusion theory, the dissolution process consists of four steps: (1) diffusion of species A (in this study, A can be Fe or Al) inside the "solid" particle from center to surface; (2) transfer of the species across the interface; (3) aqueous dissociation reaction; (4) diffusion of species A from the interface. The diffusion-like process we envision taking place within mineral dust particles is dominated by relatively fast leaching of trace species through the fissures, imperfections, and cracks of aspherical dust aggregates [*Anderson et al.*, 1996]. Since the characteristic time of step 1 is 6 or more orders of magnitude longer than other steps, the solubility of species A is controlled mainly by step 1.

2.1.1. Solving the Diffusion Equations

[8] Based on Fick's Second Law, we describe step 1 mathematically

$$\frac{\partial N_A}{\partial t} = D_A\left(\frac{\partial^2 N_A}{\partial r^2} + \frac{2}{r}\frac{\partial N_A}{\partial r}\right) \tag{1}$$

with the following initial and boundary conditions:

$$N_A(r,0) = N_0, \qquad r < R_p \tag{2}$$

$$N_A(R_p,t) = N_S \tag{3}$$

$$\left(\frac{\partial N_A}{\partial t}\right)_{r=0} = 0 \tag{4}$$

$N_A(r, t)$ is the concentration of species A; R_p is the radius of the particle; N_0 is the initial concentration; N_S is the concentration of A at the particle's surface; D_A is the diffusion coefficient.

[9] Following *Seinfeld and Pandis* [2006], we solve the diffusion equation and get the maximum solubility of species A at time t:

$$S^{max} = \int_0^t J_c^{max} = \frac{6}{\pi^2}\sum_{n=1}^{\infty}\frac{1}{n^2}\left[1 - \exp\left(-\frac{n^2\pi^2 D_A}{R_p^2}t\right)\right] \tag{5}$$

$J_c^{max}(R_p, t)$ is the diffusive flux of A outward at the particle surface assuming the concentration of A at the particle surface vanishes ($N_S = 0$), as it does for freshly condensed liquid aerosols that coat mineral dust when RH ≥ 20%. This assumption is relaxed in the next section.

2.1.2. Constraining the Solubility With Available Condensed Water

[10] Equation (5) does not limit dissolution of species A so $S^{max} \rightarrow 100\%$ after a long time. This is unrealistic because the dissolution rate will decrease as the trace concentration in

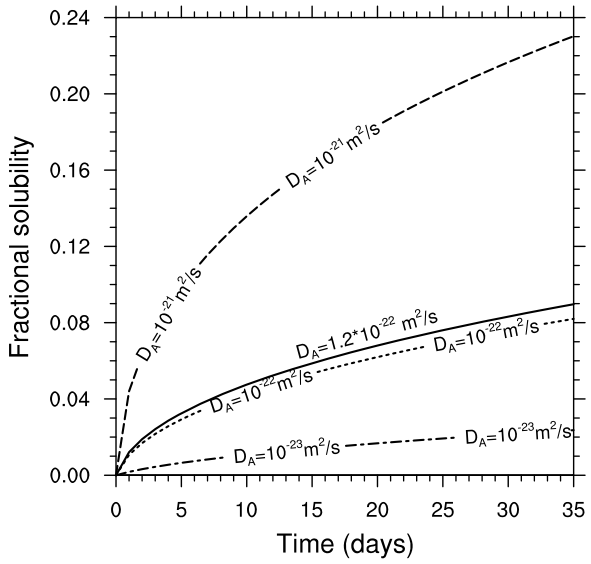

Figure 1. Evolution of fractional solubility S as a function of diffusion coefficient D_A in diffusion-controlled model.

the solution coating the dust increases. An equilibrium between the solution and the particle results when the dissolution rate reduces to zero before the particulate species A completely dissolves.

[11] *Hänel* [1976] gives an empirical relationship between the increased particle radius after the hygroscopic growth and the relative humidity:

$$r_g \approx r \times (1 - RH)^{-\epsilon} \tag{6}$$

r_g is the radius of the particle after hygroscopic growth; r is the original radius of the particle; RH is the relative humidity of the ambient air; ϵ is the experimental coefficient varies with the category of the aerosols. Here we use $\epsilon = 0.18$ for dust in the Atlantic marine environment [*Hänel*, 1976]. Thus with an atmospheric relative humidity of 80%, condensed water increases the original particle's volume by 140% and this limits the maximum solubility to 70%.

2.1.3. Determining the Diffusion Coefficient

[12] Diffusion coefficients for different geologic materials vary broadly and are largely dependent on temperature and pressure. *Watson and Baxter* [2007] show that the diffusion coefficient in minerals range from $D_A \approx 10^{-20}$ m^2 s^{-1} to 10^{-50} m^2 s^{-1} at 500°C, and typically lower at normal atmospheric temperature and pressure conditions. In our diffusion-controlled solubility model, only diffusion coefficients D_A near 10^{-22} m^2 s^{-1} yield the measured range of dust solubilities within the average dust particle lifetime in the atmosphere of ~4 days (Figure 1). We use $D_A = 1.2 \times 10^{-22}$ m^2 s^{-1} which best simulates the observed solubilities.

2.2. Conceptual Model II: Surface-Area-Controlled Dissolution

[13] The second conceptual model considers the aerosol solubility to be controlled by the exposed surface area of the dust particle and neglects any diffusive processes inside the mineral dust particles. The dissolution rate f [mol s^{-1}] is determined by the detachment rate of reaction k [mol m^{-2} s^{-1}] acting over the total surface area A [m^2] [*Stumm*, 1992]:

$$f = k \times A \tag{7}$$

Here k varies with species, pH, and temperature. For complex particles and aggregates like mineral dust, A depends on the surface roughness factor λ and the geometric surface area $s(r)$ [m^2] as:

$$A = \lambda \times s(r) \tag{8}$$

Thus for any particle, the fractional solubility S is:

$$S(r,t) = \frac{\mathrm{M} \times k \times \lambda \times s(r) \times t}{V(r) \times \rho \times C_1} \tag{9}$$

M is the molar mass of Fe [55.845 g mol^{-1}] or Al [26.982 g mol^{-1}]; t is the elapsed time of dissolution (taken here to be the atmospheric transport time); $V(r)$ is the particle volume [m^3]; $\rho = 2.5 \times 10^6$ g m^{-3} is the density of dust particles and $C_1 = 3.5\%$ is the assumed iron content in dust [*Taylor and McLennan*, 1985].

2.2.1. Choosing the Parameters

[14] During the last few decades, intensive research has been done on the mineral-water-surface-controlled dissolution process and the specified reaction rate k has been measured through both laboratory work and natural system studies for many kinds of minerals under various conditions [*Stumm*, 1992; *Brantley*, 2008]. The reaction rates of various Al-minerals range from 1.5×10^{-10} to 2.0×10^{-13} M m^2 s^{-1} at 25° and pH = 3 [*Wehrli et al.*, 1990]. Goethite/hematite are thought to be dominant Fe reservoirs in mineral dust [*Claquin et al.*, 1999; *Lafon et al.*, 2006]. Other iron-containing aluminosilicates, such as clay, contribute to soluble iron as well [*Journet et al.*, 2008]. For laboratory-ground goethite and hematite particles, an empirical relationship between the reaction rates and pH is found to be $\log(k) = -10.98 - 0.43 \times$ pH [*Cheah et al.*, 2003; *Brantley et al.*, 2006]. Although this relation is based on only goethite and hematite, it produces solubilities in agreement with observations of ambient dust if we increase k yet retain its pH-dependence by altering the relation to:

$$\log(k) = -10.13 - 0.43 \times \mathrm{pH} \tag{10}$$

Since no measured relation between the detachment rate k or the dissolution rate f and pH has been reported for Al, we also use equation (10) for Al. The soluble Al deposition flux will be calculated using Fe solubility and 8% Al content in dust.

[15] The pH values were measured before dissolution in the empirical relationship (10). What complicates the application of (10) in global models is that aerosol pH evolves continually due to aerosol solubilization [*Desboeufs et al.*, 2003] and to spatio-temporarily varying aerosol emissions and removal processes. Several cruises have found a positive correlation between solubility and the ratio of aerosol acids to dust mass [*Sato*, 2003; *Chen and Siefert*, 2004]. We approximate the acidity of dust coatings during transport

using the valence-adjusted ratios of sulfate and nitrate aerosol fluxes to dust flux at deposition:

$$\mathrm{pH}^{*} = -\log\left(\frac{F_{SO_4^{2-}} \times 2 + F_{NO_3^-}}{F_{\mathrm{dust}}^{\frac{1}{3}} \times C_2}\right) \quad (11)$$

$F_{SO_4^{2-}}$, $F_{NO_3^-}$ are the annual deposition flux fields for sulfate and nitrate estimated by *Luo et al.* [2007] using the UC Irvine global chemistry transport model (UCICTM) with an embedded aerosol equilibrium model; F_{dust} is the climatological dust deposition flux from driving the Dust Entrainment and Deposition (DEAD) model with NCEP/NCAR reanalysis for the period 1990–1999 [*Zender et al.*, 2003]; C_2 is a unitless scale factor. Since the range of dust fluxes is several orders of magnitude wider than the range of acid fluxes, we use the cubic root of dust fluxes to create a reasonable global pH distribution of the atmospheric aerosols.

[16] The surface roughness factor λ is the BET surface area (BET consists of the first initials of the authors' family names [*Brunauer et al.*, 1938]) divided by the geometric surface area $s(r)$. This factor largely depends on the weathering condition, i.e., the age and aggregation of the bulk soil. It can be as high as 620 for very old soils and less than 10 for new soils [*White et al.*, 1996]. It also depends on the type of soil and tends to increase with increasing particle size [*Anbeek*, 1992; *White et al.*, 1996]. Most roughness factor measurements are for particles larger than 10 μm, while we are most interested in long range transported particles smaller than 10 μm. We pick $\lambda = 100$ for which the computed particle specific surface areas agree well with laboratory measurements [*Brantley et al.*, 2006; *Cwiertny et al.*, 2008; *Journet et al.*, 2008] for the size range (0.1–10.0 μm) modeled here.

[17] A potential problem for this method raises when the aerosol particle is strongly acidic (e.g., pH < 1) for a very long period (e.g., on the scale of months). It is possible to get a solubility of larger than 100% following the formulas above under such extreme conditions since there is no buffer terms to reduce the dissolution rate. One possible way to eliminate this problem is to compare the concentration of Fe or Al in the solution (the liquid coating surrounding the particle) to the measured chemical activities of Al^{3+}, Fe^{3+} in water equilibrium extracts from acid mine drainage [*Sullivan et al.*, 1988; *Sposito*, 1996; *Ahum and Lavkulich*, 1998]. However, these measurements are for particles of millimeters in size or larger and therefore the measured activities are far less than the normal Fe^{3+} concentration in our calculation. Fortunately, such strong acidic condition rarely exists and 90% of dust deposits less than 10 days since emission [*Han and Zender*, 2010] so that this potential problem has little impact.

2.3. Solubility Observations

[18] Iron solubility has been measured with different techniques that are not completely mutually consistent and intercomparable. We compiled a database of iron solubility field observations to evaluate our models.

[19] Soluble iron measurements were performed from the MP01–MP09 cruises in the Pacific and Atlantic Oceans [*Johansen et al.*, 2000; *Chen and Siefert*, 2004]. Two size fractions (diameter $D < 2.5$ μm for fine fraction and $D > 2.5$ μm for coarse fraction) of ambient aerosol samples were collected using a high-volume dichotomous virtual impactor (HVDVI). Labile Fe(II), labile Fe(III) and reducible particulate Fe were operationally defined and measured by the extraction time and reagents. The total iron concentration was analyzed using inductively coupled plasma mass spectrometry after a strong-acid digestion procedure. Previous studies used both Fe(II) and labile Fe(II and III) as soluble iron to compare with model results [*Luo et al.*, 2005, 2008]. In our work, we define iron solubility for these measurements as [Fe(II)+Fe(III)]/(Total Fe)*100 for a better compatibility with other methods.

[20] Following *Sarthou et al.* [2003], the aerosol samples from RV Polarstern (ANT18-1), RRS James Clark Ross (JCR) and FS Meteor cruise M55 in the Atlantic Ocean were collected using a high volume sampler (1 m^3/min) and then separated to fine/coarse fractions at $D = 1$ μm [*Baker et al.*, 2003]. Soluble iron was extracted by leaching the aerosol sample filters in ammonium acetate buffer at pH = 4.7 for 1–2 h. The supernatant was then drawn through a 0.2 μm filter, acidified with HNO_3 and analyzed for total iron. *Luo et al.* [2008] applied a 0.5 factor when comparing Fe(II) to these measurements. In contrast, we compare to the unmodified measurements since we use total (Fe(II)+Fe(III)) labile iron.

[21] The aerosols from A16N CLIVAR cruise in the Atlantic and 2002 IOC cruise in the Pacific were measured as described in *Buck et al.* [2006, 2008a, 2008b]. Aerosol samples were collected by an automatic sector-controlled system at a flow rate of 30–50 L/min. Unlike other techniques, they measured the "instantaneous" soluble Fe and Al by quickly passing 100 mL of filtered surface seawater or unacidified DI water (pH = 5.6) through the aerosol sample filter. These correspond to their seawater soluble iron or DI water soluble iron respectively. The total iron was obtained using energy-dispersive X-ray fluorescence (EDXRF). The DI water solubility is generally higher than the seawater solubility. We find that seawater solubility is more comparable with solubilities observed from other cruises than DI solubility. Solubility data from two new Pacific CLIVAR cruises are also included in our database.

[22] Al solubility data are only available on cruises 2002 IOC and the Atlantic and Pacific CLIVAR for DI water and on cruise JCR. Hence we focus on comparing iron solubility in this work. We use the solubility in seawater from the CLIVAR and IOC cruises to constrain the parameters (D_A and k) in our conceptual models, and then we compare our model results with the remaining observations. Although these observations were made using different approaches for measuring solubility, they all share the common characteristic that they are based on a simple leaching solution not subject to iron solubility constraints [*Baker and Croot*, 2010].

2.4. Models

[23] In this work, we use the monthly mean dust deposition field obtained from driving the Dust Entrainment And Deposition (DEAD) model with 1990s observed meteorology [*Zender et al.*, 2003; *Mahowald et al.*, 1997]. The DEAD model simulates size dependent dust processes including mobilization, transport, and dry and wet deposition for particles size from 0.1–10 μm which includes most long-range transported dust. These particles are put into four size bins (0.1–1.0, 1.0–2.5, 2.5–5.0, 5.0–10.0 μm) and are assumed to be log-normally distributed within each bin [*Zender et al.*, 2003].

[24] We will compare the response of the Biogeochemical Elemental Cycling (BEC) ocean model [*Moore et al.*, 2004] with soluble Fe and Al fluxes from our spatially variable solubility models to the ecosystem response to the constant 5% solubility (the base run) used before [*Han et al.*, 2008]. The BEC ocean model couples the upper ocean ecosystem model [*Moore et al.*, 2002] and an expanded biogeochemistry module [*Doney et al.*, 2003] with the ocean circulation component of the Community Climate System Model 3.0 [*Collins et al.*, 2006]. This marine ecosystem model includes one zooplankton and four phytoplankton functional groups: coccolithophores, small phytoplankton, diatoms, and diazotrophs; key limiting nutrients: nitrate, ammonium, phosphate, iron, and silicate; sinking particulates and dissolved organic matter. In these components, the model tracks carbon, nitrogen, phosphorus, iron, silicon, oxygen and calcium carbonate and then predicts the biomass, productivity, community structure, and carbon export in the ocean ecosystem. Al cycling has been incorporated into the BEC model [*Han et al.*, 2008]. In addition, the version used here includes improvements in the iron scavenging parameterizations and the more realistic sedimentary iron source from *Moore and Braucher* [2008]. We optimized the Fe and Al scavenging coefficients for each soluble Fe and Al deposition map with all other parameter values staying identical in the three simulations. The observations of dissolved Fe and Al concentrations in the surface ocean have been summarized by *Moore and Braucher* [2008] and *Han et al.* [2008] respectively.

3. Results

3.1. Modeled Solubility for Variable Particle Sizes

[25] The predicted solubility increases with time for both conceptual models (Figures 2a–2c) and smaller particles (size bins 1 and 2, $0.1 < D < 2.5$ μm) always have higher solubilities than larger particles. Initially, the diffusion-controlled model and the surface-controlled model at pH = 3 predict similar solubilities. After ~10 days the model solubility predictions diverge. The solubility predicted by the diffusion-controlled model levels off with time due to the limited condensed water (i.e., particle coating) available. The maximum solubility predicted from the diffusion-controlled model is ~70%. The solubility predicted by the surface-area-controlled model increases linearly with time and reaches the maximum of 100% in ~60 days for the sub-micron dust (size bin 1) with coatings at pH = 3. This maximum is rarely reached during transport since 90% of dust deposits within 10 days since emission [*Han and Zender*, 2010].

[26] Iron dissolves much faster at lower pH in the surface-controlled model. At a fixed time $t = 4$ days (which is the mean dust residence time in the atmosphere), the particle is almost non-soluble at pH > 4 and solubility increases exponentially as pH decreases from 4 (Figure 2d). It takes ~10 days at pH = 3 to reach 2–15% solubility and only 30 hours at pH = 1. This is consistent with the laboratory measurements of iron solubility ranging from 6–17% for different dust source samples at pH = 1 after 30 hours [*Cwiertny et al.*, 2008].

3.2. Geographic Distribution of Solubility

[27] With size-resolved geographic dust deposition fluxes from DEAD [*Zender et al.*, 2003] and dust age at deposition from MAT [*Han and Zender*, 2010], we estimated the Fe or Al solubility in deposited dust at any location from the relation (5) between solubility, dust size and transport time, based on the diffusion-controlled conceptual model (Figure 3a). Using the climatological pH distribution estimated in *Luo et al.* [2007], we estimated the distribution of Fe solubility based on the surface-controlled conceptual model (Figure 3b). Both solubility maps show very low solubility over the continents near dust source regions such as Northern Africa, Australia and central Asia, as well as over oceanic regions downwind from dust sources such as the northern equatorial Atlantic. Both models estimate the lowest solubilities, under 0.5%, in deserts. Solubilities outside the dust source regions depend sensitively on the conceptual model, though all solubilities increase with transport time and with smaller particle sizes. All solubilities are low near to and downwind from source regions where the large particles are still abundant and the dust is young. Solubilities increase farther from source regions.

[28] The highest diffusion-based solubilities (Figure 3a) occur in the equatorial Pacific where the deposited dust age is very old (~30 days) and small dust particles dominate. Diffusion-based solubilities over most of the Atlantic are lower than 6% except the area from 5–30°S and in the far northwest. Solubilities over the Pacific are generally higher than 6% except downwind from Australian, North American, and East Asian sources. Solubilities over the Southern Ocean range from 1% to 10% depending on the proximity of the area to dust source regions.

[29] The solubility distribution estimated from the surface-area-controlled model (Figure 3b) is largely controlled by the estimated aerosol acidity, i.e., by the relative abundance of acids (sulfate and nitrate) to dust rather than the dust particle size and dust age at deposition. Solubility in and near source regions is still low due to the high dust concentration and the young dust age. But the highest solubilities occur where the estimated acid deposition fluxes are highest relative to dust deposition fluxes, e.g. southeastern Asia, western Europe, eastern North America and northern South America. The highest solubilities exceed 40%, more than twice the highest estimated solubilities from the diffusion-controlled model. The solubilities over most ocean areas range from 4–10% due to the moderate acid to dust ratio and the moderate dust age. Exceptions include the northern equatorial Atlantic and 0–70°W of the Southern Ocean where modeled solubilities are very low (less than 2%) due to being downwind of strong dust and weak pollution sources. There is only one observation near the Southern Ocean (at 52°W 43°S where solubility was measured as 4.21%) so it is difficult to assess whether the low modeled solubilities are observed in this important Fe-limited region. The modeled solubility over the northwestern Pacific exceeds 10% due to the strong pollution sources upwind. Dust solubility is quite low over pristine remote regions such as Antarctica.

3.3. Model-Data Comparisons

[30] The parameters (i.e., D_A and k) that were constrained by the cruises IOC and CLIVAR data produce widely scattered solubilities compared to observations from other cruises (Figure 4). The diffusion-controlled model does not fit the cruise data well over the Atlantic Ocean ($R = 0.07$). Most simulated solubilities are within a factor of two of the

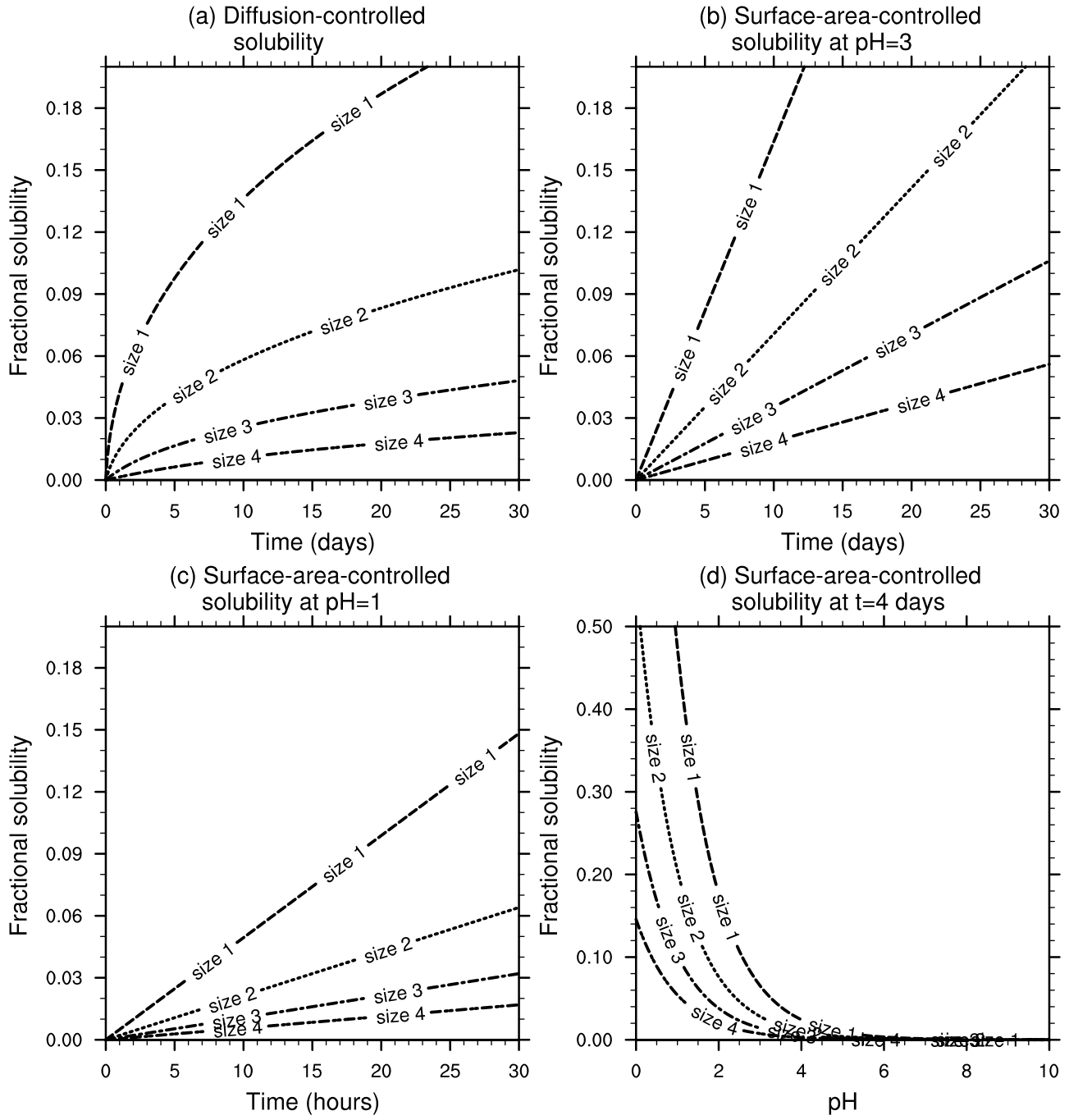

Figure 2. Fractional solubility for different size bins from (a) diffusion-controlled model in a 30-day period, (b) surface-controlled model at pH = 3 in a 30-day period, (c) surface-controlled model at pH = 1 in a 30-hour period, and (d) surface-controlled model at t = 4 days at different pH conditions.

corresponding observations, and are too high where the observed solubilities are less than 3%. The surface-controlled model simulates, on average, lower solubilities than the diffusion-controlled model. This model underestimates many points yet it captures the overall solubility pattern over the Atlantic (R = 0.57, significant at the 95% level). However, neither model captures the spatial solubility pattern over the Pacific (insignificant correlations of R = −0.04 and 0.13). Observed solubilities range from less than 1% to more than 20% across the Pacific, while our model predictions range only from 3%–10% at the same locations. An important reason for this model-data misfit in solubility could be the neglect of anthropogenic iron in our model, especially for the Pacific Ocean where the natural dust deposition is low and thus the anthropogenic source of soluble Fe is relatively more important. Neglecting anthropogenic iron may also explain the underestimate of solubility from the surface-controlled model over the Atlantic Ocean.

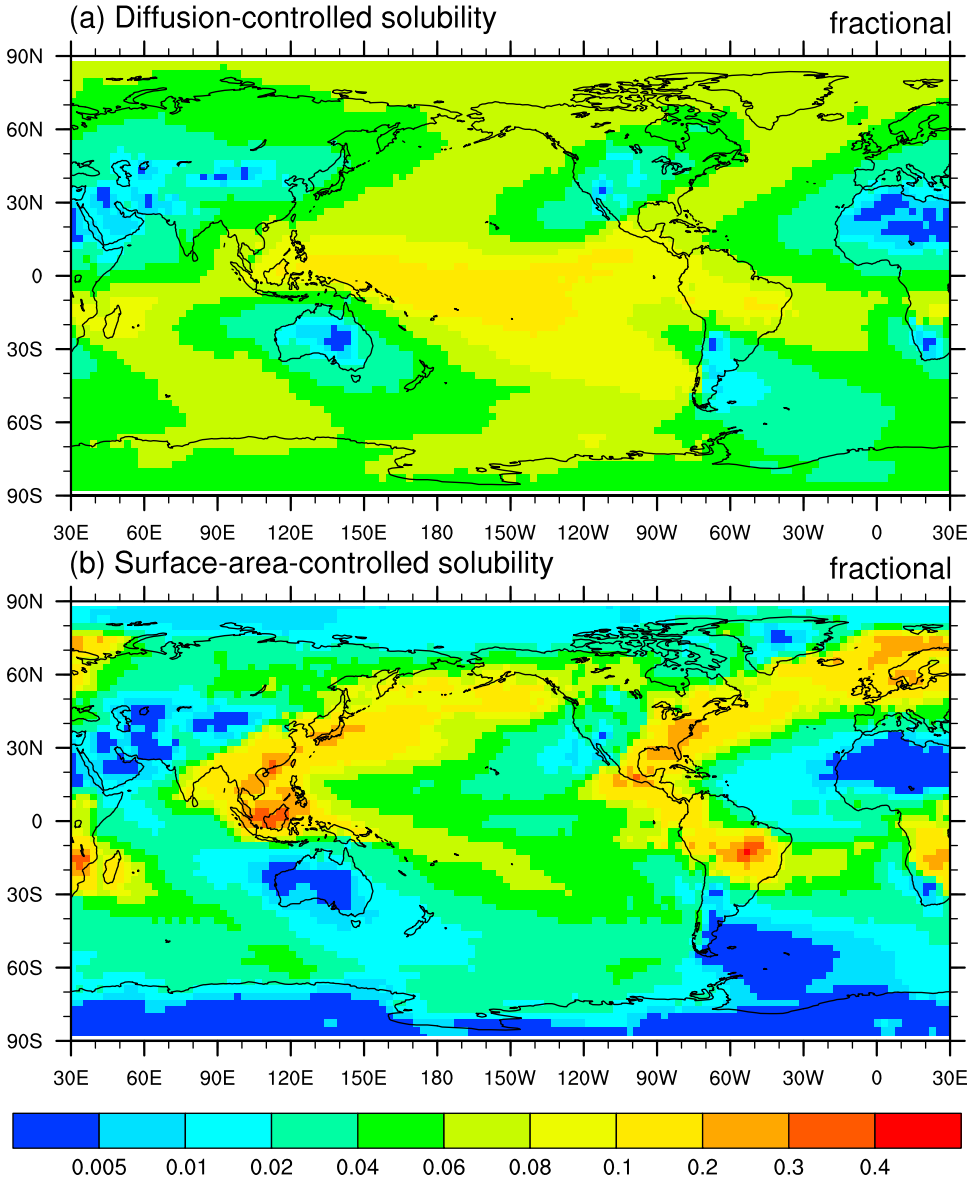

Figure 3. Geographic solubility distributions from (a) diffusion-controlled model and (b) surface-area-controlled model.

3.4. Soluble Iron Deposition Maps

[31] The two models predict similar total depositions of soluble iron to oceans (0.47–0.48 Tg/yr), and are close to the total soluble Fe (0.57 Tg/yr) deposited from a globally uniform solubility assumption of 5%. However, the distributions within ocean basins differ greatly (Figure 5 and Table 1). Both size-resolving solubility models predict higher (relative and absolute) soluble Fe fluxes to the Pacific and South Atlantic than the globally uniform solubility assumption, and lower fluxes to other oceans. The three factors responsible for this pattern are: (1) the long transit times, (2) preferential survival of small particles during transport and (3) generally high pollution-to-dust ratios on a basin-wide scale for the Pacific and South Atlantic Ocean. The diffusion-controlled model budget, when evaluated regionally, is closer than the surface-controlled model budget to the 5% solubility budget. The surface-controlled model predicts twice the soluble iron flux to the Pacific and 40% more to the South Atlantic than the 5% assumption. The soluble iron flux from the surface-controlled model is much smaller in the equatorial Atlantic than a 5% solubility flux, yet is only 20% less when averaged over the entire North Atlantic. The most dramatic difference occurs in the Southern Ocean where the surface-controlled model predicts only 15% of the soluble iron flux as the 5% solubility assumption—equivalent to a solubility of only 0.7%. This result is speculative since there are no direct iron solubility measurements in the Southern Ocean for comparison.

[32] The soluble Fe deposition maps from this study are similar to previous global studies that neglect explicit particle-size dependent processes on solubility [*Luo et al.*, 2008; *Mahowald et al.*, 2009]. This is not surprising since the dust deposition fields in these studies are predicted with

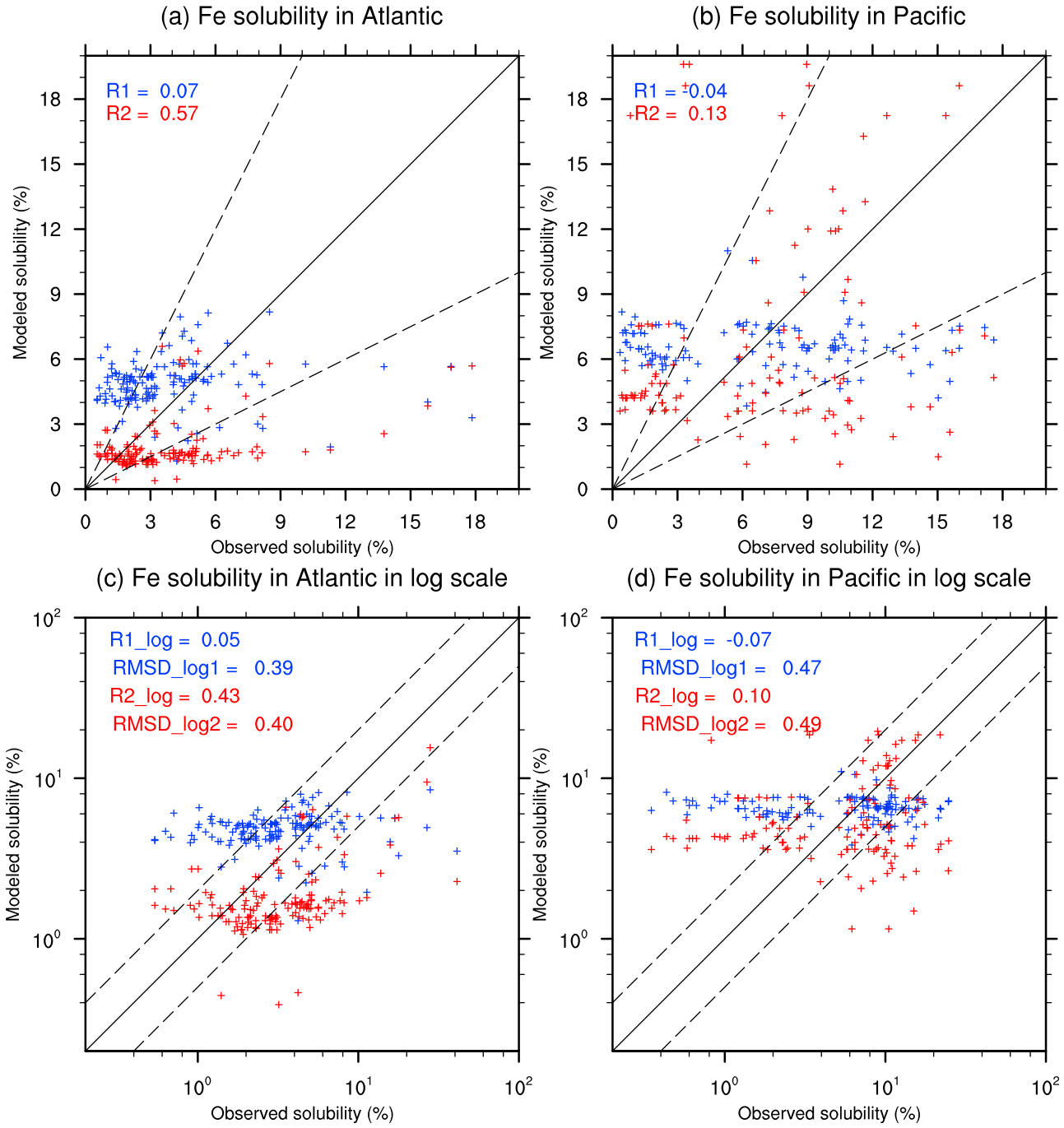

Figure 4. Fe solubilities predicted by diffusion-controlled (blue) and surface-area-controlled (red) models compared to observations (a) in the Atlantic from cruises MP01-MP09, JCR and M55, (b) in the Pacific from cruises MP01-MP09, (c) in the Atlantic Ocean on log scale, and (d) in the Pacific Ocean on log scale. Dashed lines represent factor of two agreement. RMSD is root mean square difference after logarithmic transformation.

similar physics and agree over many orders of magnitude. The global total (land+ocean) soluble iron depositions from these studies are also comparable (0.90–0.98 Tg/yr here, 0.89 Tg/yr in *Luo et al.* [2008]). However, this study predicts more than twice the soluble iron deposition to oceans than *Luo et al.* [2008] but only 1/5 of *Fan et al.* [2006]. The study also nearly quadruples the soluble iron deposition to the North Atlantic in *Luo et al.* [2008]. Though our surface-controlled model shows a slightly better correlation in the Atlantic, none of these models stands out as being the most consistent with all available observations.

3.5. Ecosystem Model Responses to Variable Solubility

[33] Overall, the dissolved Fe and Al concentrations in surface oceans simulated by the BEC model [*Moore and Braucher*, 2008; *Han et al.*, 2008] driven by the variable

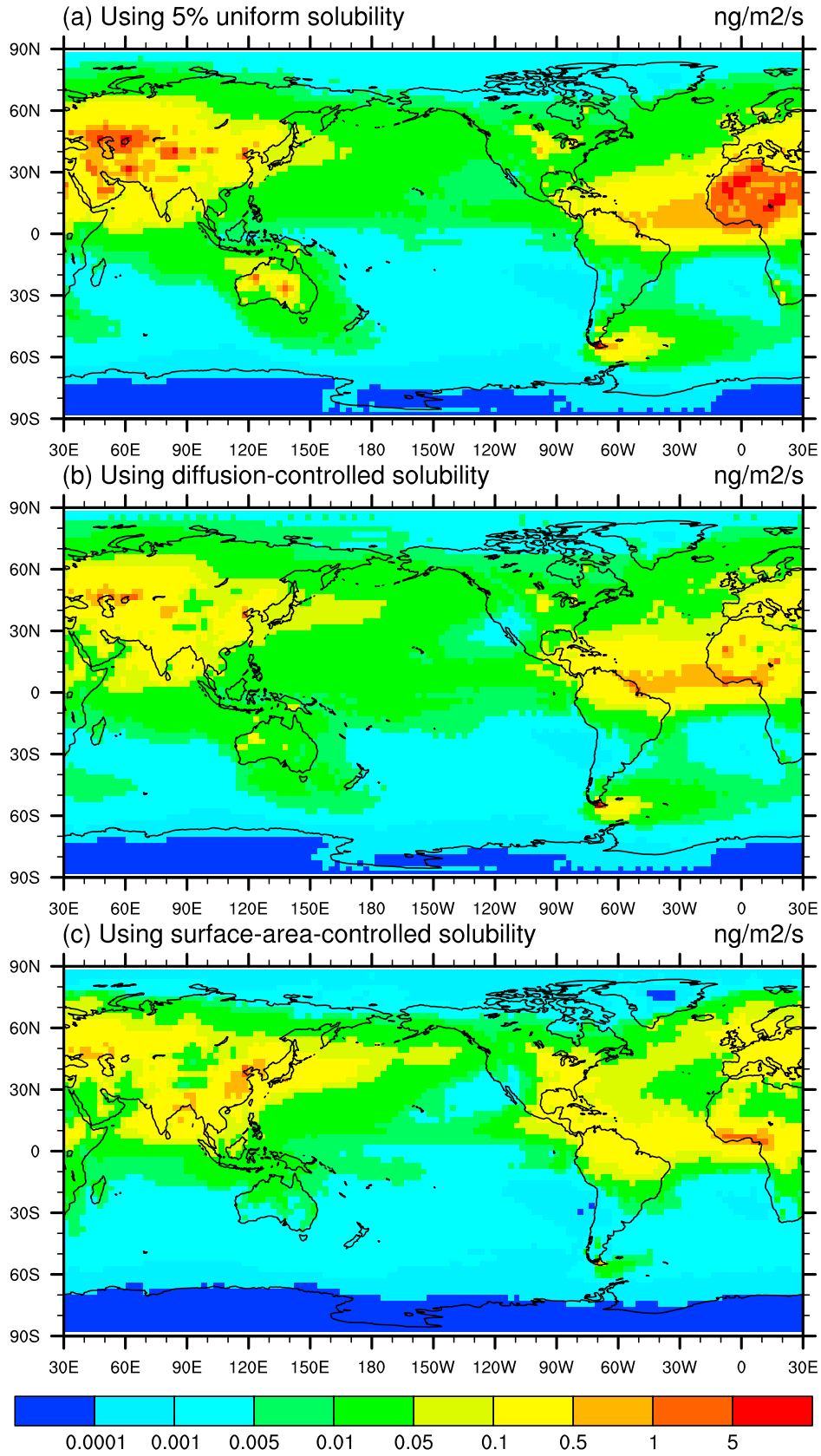

Figure 5. (a) Modeled soluble iron deposition from 5% global uniform solubility, (b) solubility predicted by diffusion-controlled conceptual model, and (c) solubility predicted by surface-controlled conceptual model. Dust field is simulated by DEAD using the 1990–1999 climatology [*Zender et al.*, 2003] and the iron content of the dust is 3.5% by weight.

Table 1. Iron Deposition, Solubility and Ecosystem Responses in Different Ocean Basins

Basins	Total Fe (Tg/yr)	Soluble Fe (Tg/yr)			Solubility (%) of Fe and Al		RMSD[a] of Dissolved Fe (nM)			RMSD of Dissolved Al (nM)		
		5%[b]	I[c]	II[d]	I	II	5%	I	II	5%	I	II
Pacific	1.24	0.062	0.082	0.124	6.6	10.1	0.501	0.514	0.616	0.529	0.476	0.601
North Atlantic	5.70	0.285	0.256	0.224	4.5	3.8	0.353	0.347	0.300	0.350	0.335	0.305
South Atlantic	0.51	0.025	0.029	0.035	5.6	7.0	0.527	0.523	0.587	0.320	0.313	0.301
Indian Ocean	1.23	0.062	0.048	0.050	3.9	4.0	0.256	0.362	0.388	0.278	0.351	0.380
Southern Ocean	1.34	0.067	0.042	0.010	3.1	0.7	0.462	0.482	0.452	0.263	0.349	0.325
Mediterranean Sea	0.53	0.026	0.010	0.015	1.8	2.8	NA	NA	NA	0.167	0.148	0.128
Oceans total[e]	11.41	0.570	0.481	0.470	4.2	4.1	0.445	0.465	0.505	0.352	0.349	0.357
Global total	50.68	2.534	0.979	0.904	1.9	1.8	NA	NA	NA	NA	NA	NA

[a]Root mean square difference, after logarithm transformation.
[b]Globally uniform 5% solubility assumption.
[c]Diffusion-controlled model.
[d]Surface-controlled model.
[e]Ocean total also includes dust deposition in marginal seas.

solubility from either our diffusion- (model I) or surface-controlled (model II) model do not fit the limited observations better than using the 5% constant solubility (Figure 6 and Table 1). The soluble Fe and Al depositions from the diffusion-controlled model produce no significantly different dissolved Fe or Al fields from the base run (comparing the absolute differences of log-transformed model predictions and observations, not statistically significant at the 0.95 level) except in the Indian Ocean, where the variable solubilities worsen the simulation. The surface-area-controlled soluble iron deposition degrades the dissolved iron comparison in the Indian Ocean and in the global ocean, and improves the

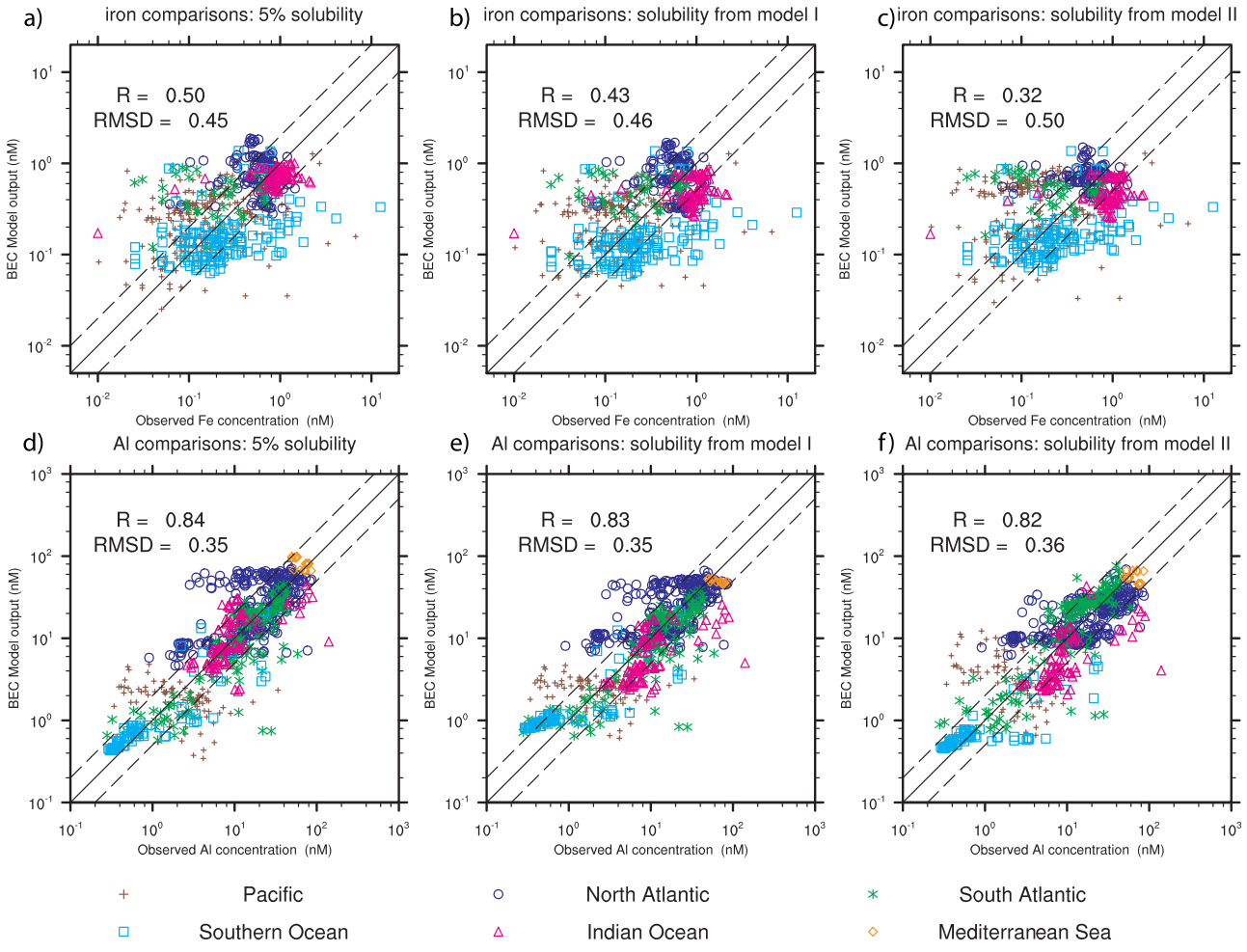

Figure 6. Dissolved Fe and Al concentrations predicted by the BEC models with different solubility fields compared to observations.

north Atlantic simulation (significant at the 0.95 level). The dissolved Al field predicted by the surface-area-controlled solubility model does not significantly change the model-observation comparison in any ocean basin except for the Indian Ocean. The fact that the predicted dissolved Al concentrations fit the data better than Fe suggests that Fe cycling in the BEC model also contributes to the discrepancy of simulated to observed iron concentrations. The advantage of using Al as a tracer is that Al cycles similarly to iron but with simpler chemistry and simpler biology. Thus better understanding of Al cycling could serve as foundation for understanding the more complex Fe cycling.

[34] The BEC appears to overestimate the surface dissolved iron in the Pacific for all solubility scenarios considered here. This overestimate may be caused by poor representation of iron solubility, dust deposition, iron sink processes or some combination of these. In the equatorial north Atlantic, the surface-controlled solubility greatly reduces the overestimate of dissolved Fe and Al in the base run (though not statistically significant for Al, it can be clearly seen from Figure 6f). The solubility from the surface-controlled model also agrees much better with observations in the North Atlantic than the 5% uniform solubility. Hence the surface-controlled solubility model performs relatively well in the North Atlantic, compared both to other models and to observations. Unfortunately, there are not field observations of solubility in some key regions where the model predictions differ most including the central, equatorial Pacific and parts of the Southern Ocean.

[35] We also checked possible ecosystem/biogeochemical impacts of variable iron solubility by comparing other BEC simulated fields among different scenarios and with observations, e.g., surface nitrate, phosphate and silicate concentrations, surface chlorophyll, total biological carbon export at 103 m, total N fixation. However, though all of these fields vary more or less at basin scale with different soluble iron inputs, none of them shows significant change globally. Since the spatial impacts of increasing soluble iron have been discussed in *Krishnamurthy et al.* [2009] using the same ecosystem model, we will not discuss this in detail here.

4. Discussion

[36] We explored two plausible relations between trace metal (i.e., Fe and Al) solubility and particle size and transport time. We developed these relations into diffusion-controlled and surface-controlled models to predict the fraction of soluble iron in dust particles. These conceptual models make numerous assumptions to simplify the complex and poorly understood dissolution processes on scales relevant to and tractable by present-day general circulation models. These models neglect many important features such as spatiotemporal variations of particle physical and chemical properties (except size), diurnal and daily variations in aerosol and pH, and cloud processing effects. Both models contain at least one parameter whose measured values range over several orders of magnitude, i.e., the diffusion coefficient for the diffusion-controlled model and the specified reaction rate and the surface roughness factor for the surface-area controlled model. In all cases we picked parameter values to yield reasonable results at the global scale but other combinations of parameter choices are just as valid (and arbitrary). In reality these parameters are not fundamentally constant but are rather functions of trace species, mineralogy, other physical and chemical properties of dust particles and environmental conditions during transport. We neglected this complexity and picked a single value or single relationship constrained by one group of observed solubility data. Although the resulting models produce solubilities in a reasonable range compared to independent measurement, these simplifications tend to eliminate natural variability, and help explain why the models do not predict the full range of observed solubility variations, particularly in the Pacific. From this initial study we can conclude that the two simplified aerosol models we examine are insufficient to remediate the biases between our model and the available observations and that chemical processing is likely playing a predominant role. In determining solubility, we have neglected and simplified processes including dust mineralogy, acidity buffering by neutralizing compounds such as ammonium, solution activity, and photochemistry. More complete and realistic physical-chemical models of solubility in conjunction with more complete atmospheric chemistry may well improve simulations of particle solubility and its evolution.

[37] Dust age at deposition is an important variable in both conceptual models. Smaller particles are usually older at deposition and therefore endure more atmospheric processing. Hence dust age at deposition reinforces the effects of particle size. Weather (wind and precipitation) during transport has significant impact on dust age, especially for smaller dust particles.

[38] More solubility observations would better constrain and improve our understanding of trace metal solubility. The current observations use different techniques that are not fully comparable with each other. These observations are geographically clustered, mostly in the North Pacific and the North Atlantic. There are few aerosol solubility measurements in the Southern Ocean, where the bio-available iron input is vital [*Krishnamurthy et al.*, 2010] and where our models diverge the most from each other and from previous studies. There are no lengthy, continual, much less climatological time series of solubility over land or oceans. In our conceptual models, all the variables including dust deposition, dust age, pH distribution change seasonally. Seasonal cycles of solubility at some fixed locations would thus provide very useful constraints on our models. Considering the difficulties and cost of sampling over open oceans, aerosol solubility measurements over continental regions, especially downwind of dust or pollution sources, would also be very useful.

[39] **Acknowledgments.** This research was supported by NSF OCE-0452972, NSF ARC-0714088, NASA NNX07AR23G and NSF OCE-0928204. We thank Alex Baker for sharing data with us. We also thank J. Randerson, N. Mahowald, C. Luo and the anonymous reviewer for suggestions to improve the model and helpful comments.

References

Ahum, M., and L. Lavkulich (1998), Speciation and solubility relationships of Al, Cu and Fe in solutions associated with sulfuric acid leached mine waste rock, *Environ. Geol.*, *38*(1), 59–68.

Anbeek, C. (1992), Surface roughness of minerals and implications for dissolution studies, *Geochim. Cosmochim. Acta*, *56*, 1461–1469.

Anderson, J. R., P. R. Buseck, T. L. Patterson, and R. Arimoto (1996), Characterization of the Bermuda tropospheric aerosol by combined

individual-particle and bulk-aerosol analysis, *Atmos. Environ.*, *30*(2), 319–338.
Arimoto, R., R. A. Duce, B. J. Ray, and U. Tomza (2003), Dry deposition of trace elements to the western North Atlantic, *Global Biogeochem. Cycles*, *17*(1), 1010, doi:10.1029/2001GB001406.
Baker, A. R., and P. L. Croot (2010), Atmospheric and marine controls on aerosol iron solubility in seawater, *Mar. Chem.*, *120*, 4–13.
Baker, A. R., and T. D. Jickells (2006), Mineral particle size as a control on aerosol iron solubility, *Geophys. Res. Lett.*, *33*, L17608, doi:10.1029/2006GL026557.
Baker, A. R., S. D. Kelly, K. F. Biswas, M. Witt, and T. D. Jickells (2003), Atmospheric deposition of nutrients to the Atlantic Ocean, *Geophys. Res. Lett.*, *30*(24), 2296, doi:10.1029/2003GL018518.
Behrenfeld, M. J., A. J. Bale, Z. S. Kolber, J. Aiken, and P. G. Falkowski (1996), Confirmation of iron limitation of phytoplankton photosynthesis in the equatorial Pacific Ocean, *Nature*, *383*, 508–511.
Boyd, P. W., et al. (2000), A mesoscale phytoplankton bloom in the polar Southern Ocean stimulated by iron fertilization, *Nature*, *407*, 695–702.
Brantley, S. L. (2008), Kinetics of mineral dissolution, in *Kinetics of Water-Rock Interaction*, edited by S. L. Brantley, J. D. Kubicki, and A. F. White, pp. 151–210, Springer, New York.
Brantley, S. L., S. Ruebush, J.-H. Jang, and M. Tien (2006), Analysis of (bio)geochemical kinetics of Fe(III) oxides, in *Methods of Investigating Microbial-Mineral Interactions*, *CMS Workshop Lectures*, vol. 14, edited by P. A. Maurice and L. A. Warren, pp. 151–210, Clay Miner. Soc., Chantilly, Va.
Brunauer, S., P. H. Emmett, and E. Teller (1938), Adsorption of gases in multimolecular layers, *J. Am. Chem. Soc.*, *60*, 309–319.
Buck, C. S., W. M. Landing, J. A. Resing, and G. T. Lebon (2006), Aerosol iron and aluminum solubility in the northwest Pacific Ocean: Results from the 2002 IOC cruise, *Geochem. Geophys. Geosyst.*, *7*, Q04M07, doi:10.1029/2005GC000977.
Buck, C. S., W. M. Landing, and J. A. Resing (2008a), Particle size and aerosol iron solubility: A high-resolution analysis of Atlantic aerosols, *Mar. Chem.*, *120*, 14–24, doi:10.1016/j.marchem.2008.11.002.
Buck, C. S., W. M. Landing, J. A. Resing, and C. I. Measures (2008b), The solubility and deposition of aerosol Fe and other trace elements in the North Atlantic Ocean: Observations from the A16N CLIVAR/CO_2 repeat hydrography section, *Mar. Chem.*, *120*, 57–70, doi:10.1016/j.marchem.2008.08.003.
Cheah, S.-F., S. M. Kraemer, J. Cervini-Silva, and G. Sposito (2003), Steady-state dissolution kinetics of goethite in the presence of desferrioxamine B and oxalate ligands: Implications for the microbial acquisition of iron, *Chem. Geol.*, *198*, 63–75, doi:10.1016/S0009-2541(02)00421-7.
Chen, Y., and R. L. Siefert (2004), Seasonal and spatial distributions and dry deposition fluxes of atmospheric total and labile iron over the tropical and subtropical North Atlantic Ocean, *J. Geophys. Res.*, *109*, D09305, doi:10.1029/2003JD003958.
Chuang, P. Y., R. M. Duvall, M. M. Shafer, and J. J. Schauer (2005), The origin of water soluble particulate iron in the Asian atmospheric outflow, *Geophys. Res. Lett.*, *32*, L07813, doi:10.1029/2004GL021946.
Claquin, T., M. Schulz, and Y. J. Balkanski (1999), Modeling the mineralogy of atmospheric dust sources, *J. Geophys. Res.*, *104*(D18), 22,243–22,256.
Collins, W. D., et al. (2006), The community climate system model version3 (CCSM3), *J. Clim.*, *19*(11), 2122–2161.
Cwiertny, D. M., J. Baltrusaitis, G. J. Hunter, A. Laskin, M. M. Scherer, and V. H. Grassian (2008), Characterization and acid-mobilization study of iron-containing mineral dust source materials, *J. Geophys. Res.*, *113*, D05202, doi:10.1029/2007JD009332.
Desboeufs, K. V., R. Losno, and J. L. Colin (2003), Relationship between droplet pH and aerosol dissolution kinetics: Effect of incorporated aerosol particles on droplet pHduring cloud processing, *J. Atmos. Chem.*, *46*, 159–172.
Doney, S. C., K. Lindsay, and J. K. Moore (2003), Global ocean carbon cycle modeling, in *Ocean Biogeochemistry: A JGOFS Synthesis*, edited by M. Fasham, pp. 217–238, Springer, Berlin.
Fan, S.-M., W. J. Moxim, and H. Levy II (2006), Aeolian input of bioavailable iron to the ocean, *Geophys. Res. Lett.*, *33*, L07602, doi:10.1029/2005GL024852.
Fung, I. Y., S. K. Meyna, I. Tegen, S. C. Doney, J. G. John, and J. K. B. Bishop (2000), Iron supply and demand in upper ocean, *Global Biogeochem. Cycles*, *14*(1), 281–295.
Grassian, V. H. (2001), Heterogeneous uptake and reaction of nitrogen oxides and volatile organic compounds on the surface of atmospheric particles including oxides, carbonates, soot and mineral dust: Implications for the chemical balance of the troposphere, *Int. Rev. Phys. Chem.*, *20*(3), 467–548.
Han, Q., and C. S. Zender (2010), Desert dust aerosol age characterized by mass-age tracking of tracers, *J. Geophys. Res.*, *115*, D22201, doi:10.1029/2010JD014155.
Han, Q., J. K. Moore, C. Zender, C. Measures, and D. Hydes (2008), Constraining oceanic dust deposition using surface ocean dissolved Al, *Global Biogeochem. Cycles*, *22*, GB2003, doi:10.1029/2007GB002975.
Hand, J. L., N. M. Mahowald, Y. Chen, R. L. Siefert, C. Luo, A. Subramaniam, and I. Fung (2004), Estimates of atmospheric-processed soluble iron from observations and a global mineral aerosol model: Biogeochemical implications, *J. Geophys. Res.*, *109*, D17205, doi:10.1029/2004JD004574.
Hänel, G. (1976), The properties of atmospheric aerosol particles as functions of the relative humidity at thermodynamic equilibrium with the surrounding moist air, *Adv. Geophys.*, *19*, 73–188.
Jickells, T. D., and L. J. Spokes (2001), Atmospheric iron inputs to the oceans, in *The Biogeochemistry of Iron in Seawater*, edited by D. R. Turner and K. A. Hunter, pp. 85–121, John Wiley, Chichester, U. K.
Jickells, T., T. Church, A. Veron, and R. Arimoto (1994), Atmospheric inputs of manganese and aluminium to the Sargasso Sea and their relation to surface water concentrations, *Mar. Chem.*, *46*, 283–292.
Jickells, T. D., et al. (2005), Global iron connections between desert dust, ocean biogeochemistry and climate, *Science*, *308*(5718), 67–71, doi:10.1126/science.1105959.
Johansen, A. M., and J. M. Key (2006), Photoreductive dissolution of ferrihydrite by methanesulfinic acid: Evidence of a direct link between dimethylsulfide and iron-bioavailability, *Geophys. Res. Lett.*, *33*, L14818, doi:10.1029/2006GL026010.
Johansen, A. M., R. L. Siefert, and M. R. Hoffmann (2000), Chemical composition of aerosols collected over the tropical North Atlantic Ocean, *J. Geophys. Res.*, *105*(D12), 15,277–15,312.
Journet, E., K. V. Desboeufs, S. Caquineau, and J.-L. Colin (2008), Mineralogy as a critical factor of dust iron solubility, *Geophys. Res. Lett.*, *35*, L07805, doi:10.1029/2007GL031589.
Krishnamurthy, A., J. K. Moore, N. Mahowald, C. Luo, S. C. Doney, K. Lindsay, and C. S. Zender (2009), Impacts of increasing anthropogenic soluble iron and nitrogen deposition on ocean biogeochemistry, *Global Biogeochem. Cycles*, *23*, GB3016, doi:10.1029/2008GB003440.
Krishnamurthy, A., J. K. Moore, N. Mahowald, C. Luo, and C. S. Zender (2010), Impacts of atmospheric nutrient inputs on marine biogeochemistry, *J. Geophys. Res.*, *115*, G01006, doi:10.1029/2009JG001115.
Lafon, S., I. N. Sokolik, J. L. Rajot, S. Caquineau, and A. Gaudichet (2006), Characterization of iron oxides in mineral dust aerosols: Implications for light absorption, *J. Geophys. Res.*, *111*, D21207, doi:10.1029/2005JD007016.
Luo, C., N. M. Mahowald, N. Meskhidze, Y. Chen, R. L. Siefert, A. R. Baker, and A. M. Johansen (2005), Estimation of iron solubility from observations and a global aerosol model, *J. Geophys. Res.*, *110*, D23307, doi:10.1029/2005JD006059.
Luo, C., C. S. Zender, H. Bian, and S. Metzgerc (2007), Role of ammonia chemistry and coarse mode aerosols in global climatological inorganic aerosol distributions, *Atmos. Environ.*, *41*, 2510–2533, doi:10.1016/j.atmosenv.2006.11.030.
Luo, C., N. Mahowald, T. Bond, P. Y. Chuang, P. Artaxo, R. Siefert, Y. Chen, and J. Schauer (2008), Combustion iron distribution and deposition, *Global Biogeochem. Cycles*, *22*, GB1012, doi:10.1029/2007GB002964.
Mahowald, N. M., P. J. Rasch, B. E. Eaton, S. Whittlestone, and R. G. Prinn (1997), Transport of ^{222}radon to the remote troposphere using the model of atmospheric transport and chemistry and assimilated winds from ECMWF and the National Center for Environmental Prediction/NCAR, *J. Geophys. Res.*, *102*(D23), 28,139–28,151.
Mahowald, N. M., A. R. Baker, G. Bergametti, N. Brooks, R. A. Duce, T. D. Jickells, N. Kubilay, J. M. Prospero, and I. Tegen (2005), Atmospheric global dust cycle and iron inputs to the ocean, *Global Biogeochem. Cycles*, *19*, GB4025, doi:10.1029/2004GB002402.
Mahowald, N. M., et al. (2009), Atmospheric iron deposition: Global distribution, variability, and human perturbations, *Annu. Rev. Mar. Sci.*, *1*, 245–278, doi:10.1146/annurev.marine.010908.163727.
Martin, H. B., and S. E. Fitzwater (1988), Iron deficiency limits phyoplankton growth in the north–east Pacific subarctic, *Nature*, *331*, 341–343.
Measures, C. I., and S. Vink (2000), On the use of dissolved aluminum in surface waters to estimate dust deposition to ocean, *Global Biogeochem. Cycles*, *14*(1), 317–327.
Measures, C. I., T. Sato, S. Vink, S. Howell, and Y. H. Li (2010), The fractional solubility of aluminium from mineral aerosols collected in Hawaii and implications for atmospheric deposition of biogeochemically important trace elements, *Mar. Chem.*, *120*, 144–153.
Moore, J. K., and O. Braucher (2008), Sedimentary and mineral dust sources of dissolved iron to the world ocean, *Biogeosciences*, *5*, 631–656.

Moore, J. K., S. C. Doney, J. A. Kleypas, D. M. Glover, and I. Y. Fung (2002), An intermediate complexity marine ecosystem model for the global domain, *Deep Sea Res., Part II*, *49*, 403–462.

Moore, J. K., S. C. Doney, and K. Lindsay (2004), Upper ocean ecosystem dynamics and iron cycling in a global three-dimensional model, *Global Biogeochem. Cycles*, *18*, GB4028, doi:10.1029/2004GB002220.

Prospero, J. M., R. T. Nees, and M. Uematsu (1987), Deposition rate of particulate and dissolved aluminum derived from saharan dust in precipitation at miami, florida, *J. Geophys. Res.*, *92*, 14,723–14,731.

Sarthou, G., et al. (2003), Atmospheric iron deposition and sea-surface dissolved iron concentrations in the eastern Atlantic Ocean, *Deep Sea Res., Part I*, *50*, 1339–1352, doi:10.1016/S0967-0637(03)00126-2.

Sato, T. (2003), The fractional solubility of aluminum from atmospheric aerosols, Master's thesis, Univ. of Hawai'i at Mānoa, Honolulu.

Seinfeld, J. H., and S. N. Pandis (2006), *Atmospheric Chemistry and Physics*, 2nd ed., John Wiley, Hoboken, N. J.

Shi, Z., M. D. Krom, S. Bonneville, A. R. Baker, T. D. Jickells, and L. G. Benning (2009), Formation of iron nanoparticles and increase in iron reactivity in mineral dust during simulated cloud processing, *Environ. Sci. Technol.*, *43*, 6592–6596.

Shi, Z., S. Bonneville, M. D. Krom, K. S. Carslaw, T. D. Jickells, A. R. Baker, and L. G. Benning (2011a), Iron dissolution kinetics of mineral dust at low pH during simulated atmospheric processing, *Atmos. Chem. Phys.*, *11*, 995–1007, doi:10.5194/acp-11-995-2011.

Shi, Z., et al. (2011b), Influence of chemical weathering and aging of iron oxides on the potential iron solubility of Saharan dust during simulated atmospheric processing, *Global Biogeochem. Cycles*, *25*, GB2010, doi:10.1029/2010GB003837.

Sholkovitz, E. R., P. N. Sedwick, and T. M. Church (2009), Influence of anthropogenic combustion emissions on the deposition of soluble aerosol iron to the ocean: Empirical estimates for island sites in the North Atlantic, *Geochim. Cosmochim. Acta*, *73*, 3981–4003.

Siefert, R. L., S. O. Pehkonen, Y. Erel, and M. R. Hoffmann (1994), Iron photochemistry of aqueous suspensions of ambient aerosol with added organic-acids, *Geochim. Cosmochim. Acta*, *58*(15), 3271–3279.

Siefert, R. L., A. M. Johansen, and M. R. Hoffmann (1999), Chemical characterization of ambient aerosol collected during the southwest monsoon and intermonsoon seasons over the Arabian Sea: Labile-Fe(II) and other trace metals, *J. Geophys. Res.*, *104*, 3511–3526.

Sposito, G. (1996), *The Environmental Chemistry of Aluminum*, 2nd ed., CRC Press, Boca Raton, Fla.

Stumm, W. (1992), *Chemistry of the Solid-Water Interface*, John Wiley, New York.

Sullivan, P. J., K. J. Reddy, and J. L. Yelton (1988), Solubility relationships of aluminum and iron minerals associated with acid mine drainage, *Environ. Geol. Water Sci.*, *11*(3), 283–287.

Taylor, S. R., and S. M. McLennan (1985), *The Continental Crust: Its Composition and Evolution*, Blackwell, Oxford, U. K.

Watson, E. B., and E. F. Baxter (2007), Diffusion in solid-Earth systems, *Earth Planet. Sci. Lett.*, *253*, 307–327, doi:10.1016/j.epsl.2006.11.015.

Wedephohl, K. H. (1995), The compositon of the continental crust, *Geochim. Cosmochim. Acta*, *59*(7), 1217–1232.

Wehrli, B., E. Wieland, and G. Furrer (1990), Chemical mechanisms in the dissolution kinetics of minerals: The aspect of active sites, *Aquat. Sci.*, *52*(1), 3–31.

White, A. F., A. E. Blum, M. S. Schulz, T. D. Bullen, J. W. Harden, and M. L. Peterson (1996), Chemical weathering rates of a soil chronosequence on granitic alluvium: I. Quantification of mineralogical and surface area changes and calculation of primary silicate reaction rates, *Geochim. Cosmochim. Acta*, *60*(14), 2533–2550.

Zender, C. S., H. Bian, and D. Newman (2003), Mineral Dust Entrainment and Deposition (DEAD) model: Description and 1990s dust climatology, *J. Geophys. Res.*, *108*(D14), 4416, doi:10.1029/2002JD002775.

Zhu, X., J. M. Prospero, F. J. Millero, D. L. Savoie, and G. W. Brass (1992), The solubility of ferric ion in marine mineral aerosol solutions at ambient relative humidities, *Mar. Chem.*, *38*, 91–107.

Zhuang, G., Z. Yi, R. A. Duce, and P. R. Brown (1992), Link between iron and sulphur cycles suggested by detection of Fe(II) in remote marine aerosols, *Nature*, *355*, 537–539.

Zuo, Y., and J. Holgné (1992), Formation of hydrogen peroxide and depletion of oxalic acid in atmospheric water by photolysis of iron(III)-oxalato complexes, *Environ. Sci. Technol.*, *26*, 1014–1022.